VII. PLASMA PHYSICS*

Prof. S. C. Brown	J. D. Coccoli	J. C. Ingraham
Prof. G. Bekefi	F. X. Crist	J. J. McCarthy
Prof. D. R. Whitehouse	H. Fields	W. J. Mulligan
V. Arunasalam	E. W. Fitzgerald, Jr.	J. J. Nolan, Jr.
C. D. Buntschuh		R. E. Whitney

A. FAR INFRARED INTERFEROMETER FOR THE MEASUREMENT OF HIGH ELECTRON DENSITIES

1. Introduction

The electron concentration of a plasma can be deduced from the measured phase change Φ suffered by an electromagnetic wave in its passage through the medium. When the radiation traverses a homogeneous plasma of thickness L, the phase change is

$$\Phi = (2\pi L/\lambda)[1 - \mathrm{Re}\ \mu].\tag{1}$$

Here, λ is the wavelength of the radiation and Re μ is the real part of the refractive index of the plasma. When the plasma is not acted upon by an externally applied magnetic field, the complex refractive index[1] is, to a good approximation, given by

$$\mu^2 = 1 - \left(\frac{\omega_p}{\omega}\right)^2 \left[\frac{1}{1 + (\nu/\omega)^2} - j\frac{(\nu/\omega)}{1 + (\nu/\omega)^2}\right].\tag{2}$$

Here, ω is the frequency of the radiation (expressed in radians per second), ν is the collision frequency for momentum transfer of electrons with atoms or ions, and ω_p is the plasma frequency used in defining the electron concentration N.

$$\omega_p = [Ne^2/m\epsilon_o]^{1/2} \quad \text{in mks units}$$
$$= 56.45\ \sqrt{N} \quad \text{rad/sec.}\tag{3}$$

At low frequencies or high electron densities, the radiation suffers large reflections at the plasma boundaries, and generally the maximum density that can be measured by interferometric methods is determined by the condition $\omega_p/\omega < 1$. The minimum density that can be measured is governed by the sensitivity of the interferometer to small changes in Φ. With available microwave generators (which put out radiation with $\omega \lesssim 2\pi \times 1.5 \times 10^{11}$ rad/sec, $\lambda \gtrsim 2 \times 10^{-3}$ m), the maximum electron density that can be

measured is approximately 3×10^{20} m^{-3}. On the other hand, interferometers that operate at optical wavelengths[2] become insensitive at electron densities that are less than approximately 10^{22} m^{-3}.

The present experiment is designed to bridge the gap between $n \approx 10^{20}$ m^{-3} and $n \approx 10^{22}$ m^{-3}, a range in which techniques for measurement of electron densities are lacking. A far infrared interferometer having incoherent radiation of a wavelength of 3×10^{-4} m, ($\omega = 2\pi \times 10^{12}$ rad/sec),has been designed which is able to measure densities of plasma for which 10^{22} L > NL $\gtrsim 10^{19}$ m^{-2}. The instrument was tested on a plasma over a range of densities from 10^{18} m^{-3} to 3×10^{19} m^{-3}, and good agreement was obtained with three other independent methods of measuring the density.

In deriving the density N from the measured phase change Φ, we neglected the effect of the electron collisions. This is justified, provided that $(\nu/\omega) \ll 1$, an inequality that is well satisfied in many plasmas. We then find from Eq. 2 that

$$\text{Re } \mu = [1-(\omega_p/\omega)^2]^{1/2}. \tag{4}$$

Substituting Eq. 4 in Eq. 1 and allowing for the fact that the plasma density may vary with position along the ray s, we obtain

$$\Phi = (2\pi/\lambda) \int_0^L \left[1-\left(1-\omega_p^2(s)/\omega^2\right)^{1/2}\right] ds. \tag{5}$$

We can now expand the integrand of Eq. 5 in powers of $(\omega_p/\omega)^2$. At densities for which terms of order $(\omega_p/\omega)^4$ and higher can be neglected (a good approximation for densities less than 5×10^{21} m^{-3}), we find from Eqs. 3 and 5 that

$$\Phi \text{ (radians)} = 8.45 \times 10^{-19} \int_0^L N(s) \, ds, \tag{6}$$

so that the average density is proportioanl to Φ.

The wave not only experiences a change in phase, but it is also attenuated in its passage through the plasma. Calculations show that the intensity of the ray decreases exponentially as $\exp - \int_0^L \alpha \, ds$, where α, obtained from Eq. 2, is given by

$$\alpha = \frac{1}{\text{Re } \mu} \left(\frac{2\pi}{\lambda}\right) \left(\frac{\omega_p}{\omega}\right)^2 \left(\frac{\nu}{\omega}\right) \tag{7}$$

$$= 2.69 \times 10^{-31} \frac{N\nu}{\text{Re } \mu} \text{ m}^{-1}.$$

Thus, when the average value of αL is small compared with unity, the attenuation of the radiation is negligible; such was the case in the plasmas that we used.

When the plasma under study is subjected to an external magnetic field of strength B, the foregoing results regarding Φ and a remain valid, provided that the electron-cyclotron frequency $\omega_b = eB/m$ is small compared with ω. This leads to the requirement that $B \ll 30$ Weber's meter^{-2}.

2. Gerneral Description of the Interferometer

A schematic diagram of the instrument is shown in Fig. VII-1. The infrared source is a high-pressure mercury arc lamp (General Electric No. H4AB). The arc is focused by a small rectangular mirror (3.2×3.5 cm) onto a large spherical mirror M, and a transmission grating G1 is mounted on a sliding mounting in the path of the light. The grating produces a series of images; if the light is monochromatic, the images are distributed on the plane of the mirror according to the equation

$$n\lambda = d \sin \theta, \tag{8}$$

where d is the grating spacing, $n = 0, \pm 1, \pm 2 \ldots$ is the order of diffraction, and θ is the angular displacement of the nth image measured relative to the optical axis of the instrument. In the instrument the only orders used are $n = \pm 1$. The zero order is removed by a plane angle mirror covering the center portion of the large spherical mirror M. The second and higher orders fall outside the physical dimensions of M.

Mirror M with radius of curvature R has its center of curvature coincident with the plane of the grating G1. The two images $n = 1$ and $n = -1$, focused on M and separated by a distance $D = 2R \tan \theta$, are coherent light sources and they produce an interference pattern. The interference pattern consists of a series of sinusoidal fringes.
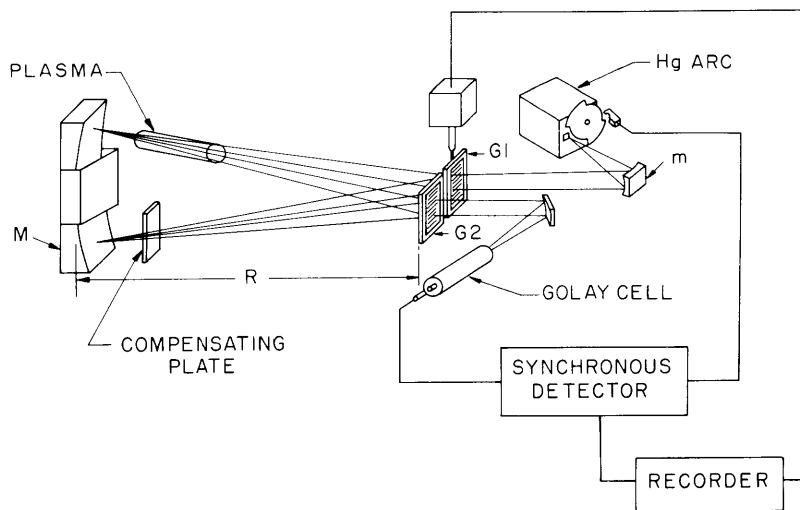

Fig. VII-1. Schematic diagram of the interferometer.

When the fringes are observed in the plane of G1 (at a distance R from the mirror), their intensity peaks are separated by a distance $x = \lambda R/D$. Since $D = 2R \tan \theta$, we obtain from Eq. 8 the fact that $X \approx \lambda/2\theta = d/2$. Hence the interference pattern has a spatial period equal to twice the grating constant, and the image of the grating has twice the density of grating elements compared with the physical grating.

The grating G1 is blazed to give maximum intensity in the +1 and -1 orders. A second grating G2, identical to G1 and coplanar with the latter, receives the radiation from the two virtual sources positioned in the plane of M. As a result of the blazing, one-half the radiation from each virtual source transmitted through G2 is refracted axially and then focused on the diamond window of a Golay detector.[3] The remaining one half of the radiation is diffracted and is lost from the system.

If the two diffraction gratings are placed identically relative to the axis of the optical system, the radiation from the two virtual sources has equal optical path lengths, and the waves transmitted through G2 and refracted toward the Golay cell interfere constructively. Thus a maximum of intensity is observed at the output from the Golay cell. If, on the other hand, G1 is displaced in a vertical plane (see Fig. VII-1) by a distance equal to one-quarter the grating spacing (d/4), the output from the Golay cell is a minimum. In the instrument G1 is driven by a motor and the output signal from the detector is displayed on a recorder. The recorder trace is a sine curve if the output signal is plotted on the Y coordinate and time on the X coordinate. If a plasma is introduced into one beam of the interferometer, the effect of its index of refraction is to shift the phase of this sine curve. This shift is then related to the phase change Φ of Eq. 1, and the electron density is computed from Eq. 6. (Note that the beam traverses the plasma twice, so that the path length of the ray L is twice the physical length of the medium.) Alternatively, if the X coordinate measures the mechanical displacement of the grating G1 and the Y coordinate measures the output signal from the Golay detector, a Lissajous figure is drawn on the X-Y recorder. The phase shift Φ produced by the plasma is then measured by the change of this Lissajous figure. Both methods have been used in this interferometer.

The poor time stability of a Golay cell and its inherent fluctuations require synchronous detection of the infrared radiation. A rotating segmented wheel drops the light coming from the arc source; the signal from the Golay cell is amplified, detected synchronously relative to a reference voltage from the chopper, and integrated. The rate at which the grating G1 is driven is made consistent with the integration time of the synchronous detector.

Table VII-1 lists the optical constants and dimensions of the interferometer.

Table VII-1. Optical constants and dimensions of the
interferometer.

Cross section of the infrared beam incident on G1	8 sq cm
Grating size of G1 and G2	2. 7 cm × 5. 3 cm
Grating constant d	0. 147 cm
Diffraction angle θ	12°
Refractive index of polyethylene gratings (μ_p)	1. 5
Radius of curvature of mirror M	61 cm
Size of mirror M	30 cm × 7. 6 cm
Chopping rate of beam	15 cps
Response time of synchronous detector	9 sec
Drive on grating G1	6. 5-13 minutes per cm

3. Details of the Design

a. Gratings

Successful operation of the interferometer largely depends upon the excellence of
the grating construction. There are very few substances that are suitable for trans-
mitting 300-μ radiation, and the only substance we were able to use for grating material
was polyethylene sheets. To obtain sufficient intensity the grating must be blazed to
put the first order at the diffraction angle given by the grating spacing. The physical
characteristics of the gratings were the following. They were made on 0.025-cm
thick polyethylene sheets, grating spacing d = 0. 147 cm, and the blazing was accom-
plished by making the lines triangular in shape with the prism angle a = 21.5°. This
value of a is consistent with the requirements that when parallel light is incident nor-
mally on the base of a prism of refractive index μ_p, the light is refracted at an angle θ
given by the relation

$$\tan a = \frac{\sin \theta}{n - \cos \theta}.$$

(9)

The gratings were made by milling a master of brass amd pressing out the poly-
ethylene gratings under pressure and heat; the brass master plate was so designed that
the proper grating spacing would be pressed into the polyethylene sheet after it had
returned to room temperature. The fraction of the incident radiation absorbed by each
grating was less than 15 per cent.

b. Source

There are few substances that efficiently transmit 300-μ radiation. Most of the
design features of this plasma interferometer are dictated by this fact. Glass is opaque
to this radiation; it was, therefore, necessary to remove the outer glass envelope of
the G. E. H4AB mercury arc light that was used as a light source for this instrument.
Since fused quartz transmits very poorly in this wavelength region, much of the desired
radiation produced by the mercury are lamp did not get out of the source even after the
glass envelope was removed. Indeed, a study of the spectral distribution of the radia-
tion shows[4] a fairly large fall-off in intensity at a wavelength around 300 μ.

c. Radiation Filters

A blazed transmission grating has the disadvantage that both the 300-μ radiation
and radiation of many other unwanted wavelengths are refracted in approximately the
same direction by the grating prisms. Therefore, the virtual images at n = ±1 located
on mirror M are no longer monochromatic. Although only one wavelength λ produces
an interference pattern with a given periodicity, large amounts of radiation of other
wavelengths cause a distortion of the sinusoidal output from the Golay detector. Par-
ticularly objectionable are wavelengths that give rise to higher-order spectra (λ = 150 μ,
100 μ, etc.).

Wavelengths below 100 μ were removed by a millimeter-thick filter of black poly-
ethylene placed in front of the Golay-cell window. An appropriate thickness of mica
was used to discriminate against 150-μ radiation. Mica, although it is not a good trans-
mitter of 300-μ radiation, can be produced in very thin sheets and has the advantage
of being a strong absorber for radiation of 150 μ, while allowing a reasonable frac-
tion of 300-μ radiation to pass through it.[4] Higher-order spectra passing through
the interferometer can be easily seen as distortions of the sine-wave output on the
Golay detector. If a fairly large amount of 150-μ radiation is present, the fact
is indicated by a superposition of large peaks, appearing on the sine wave.
This is illustrated in Fig. VII-2a. The most sensitive test for removal of the
higher orders of shorter wavelengths turned out to be to adjust the thick-
ness of the mica absorber experimentally so that the sine-wave output from
the Golay cell had symmetrical amplitudes corresponding to a spatial periodi-
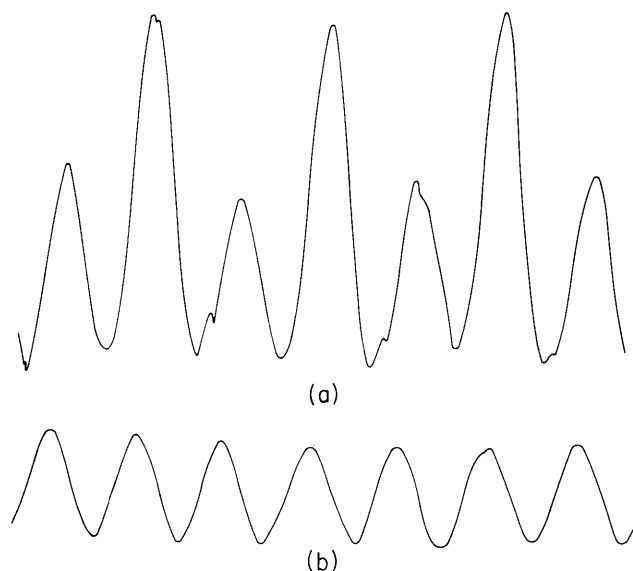city equal to d/2.

Fig. VII-2. Response of interferometer in absence of a plasma. (a) Poorly filtered (with .018-cm mica). (b) Well-filtered (with .025-cm mica).

d. Bandwidth Problem

Even when much of the unwanted radiation is removed by filter, there is still a broad band of radiation around 300 μ which can pass through the interferometer. A large bandwidth renders the calculation of the electron density from the measured phase shift meaningless. Furthermore, the plasma is a highly dispersive medium (note from Eqs. 2 and 5 that Φ is approximately proportional to the wavelength), and different wavelengths give rise to different phase shifts in the interference pattern which lead to a blurring of the sinusoidal output from the interferometer.

The bandwidth is determined primarily by the size of the virtual images that are allowed to interfere with one another. In the interferometer the bandwidth could be varied by blocking off portions of the mirror M with different sizes of masks placed symmetrically relative to the optical axis of the instrument.

Differentiating Eq. 8, we find that the fractional bandwidth, defined as BW = $\Delta\lambda/\lambda$, is given by

$$BW = \Delta\theta/\tan\theta, \tag{10}$$

where $\Delta\theta$ is the angular size that the aperture in the mask subtends at the center of curvature of mirror M. In the majority of the experiments the physical opening in the mask was 2.6 sq cm, and this gives BW $\approx$ 0.2.

When a plasma is introduced, the sinusoidal fringe pattern for one wavelength λ is displaced spatially relative to the pattern for a neighboring wavelength $\lambda \pm \Delta\lambda$. The

output of the Golay detector is the sum of the intensities over all wavelengths within the bandwidth given by Eq. 10. When the maxima of one fringe pattern (at wavelength λ) fall on the minima of the pattern for $\lambda + \Delta\lambda$, the fringes disappear and the Golay cell registers a flat output. Calculations show that for this not to happen, we must satisfy the approximate inequality

$$\Phi \times (BW) < 1, \tag{11}$$

where Φ is the total phase change caused by the plasma and is twice the value given by Eq. 6.

Inequality (11) imposes rather serious limitations on the maximum density that can be measured for a given bandwidth. Setting $\Phi \times (BW) = 1$ and $BW = 0.2$, we see that Φ must be less than 5 radians. We then find from Eq. 6 that the maximum measurable density of a uniform plasma, 1 cm thick, is approximately 4×10^{20} m^{-3}. A reduction of the bandwidth is accompanied by a reduction in the signal-to-noise ratio that is already bad for the Golay detector. Note, however, that at large electron densities Φ is large and thus a deterioration of the signal-to-noise ratio is not disastrous. In the present arrangement a reduction in bandwidth by a factor of 2 or 3 can be tolerated, provided that Φ is large.

e. Compensating Plate

Attenuation of radiation in passing in and out of the plasma tube is an unavoidable drawback that must be minimized by the use of proper windows in the plasma tube. In the particular model of the interferometer described here, the radiation had to pass through each of two windows twice, and crystal quartz was the only satisfactory window material that we were able to use. Crystal-quartz windows, 5 cm in diameter and 0.15 cm thick, were used. Since crystal quartz cannot be fused either to Pyrex or fused quartz, materials used as envelopes of plasma tubes, the infrared windows were held in place by a rubber O-ring assembly.

Whatever thickness and type of material were used for the windows of the plasma tubes, they were also introduced into the free arm of the interferometer as a compensating plate. Without the compensating plate, either no fringe pattern or a very poor pattern was observed. The compensating plate has a twofold purpose. It compensates for the attenuation suffered by the radiation in traversing the plasma tube, and what is found to be more important, it compensates for the fact that radiation, which is neither perfectly parallel nor monochromatic, suffers very large phase changes in traversing the crystal-quartz windows. Indeed, in measuring very large plasma densities it may prove necessary to compensate particularly for the phase change caused by the plasma. The magnitude of the compensation could then be used to find Φ and, hence, N.

f. Detection and Recording

The principal drawback of this initial model of an infrared interferometer is the Golay detector. This is a pneumatic device that is sensitive to $\sim10^{-11}$ watt and is so slow that it is good essentially only for steady-state plasmas. It is a noisy detector and is beset by large drifts of its zero setting. We chose this detector with the knowledge that better solid-state detectors were available,[5] but feeling that if we could make this simple detector work, then the problem of refinement to higher sensitivity and faster operation would be ensured. The synchronous detector and integrator that we used is essentially the same as that described by R. H. Dicke.[6] The sensitivity of the device, that is, the minimum detectable infrared signal, is inversely proportional to the product of the bandwidth and the square root of the time constant of the instrument. We note that this requirement on bandwidth is exactly opposite to that required for a good fringe pattern (see Eq. 11). The time of observation was determined by three times: the rate at which the grating was driven, the inherent time constant of the Golay detector, and the integration time of the Dicke amplifier. Provided that the first two times are made consistent with it, the over-all time constant can be controlled by the integration time of the electronic circuit, and we were successful in taking satisfactory data with integration times varying from 1 to 20 seconds.

Several methods of recording the data were tried successfully. One straightforward method, as mentioned previously, is to record the sine-wave output of amplitude as a function of time on the X-Y recorder, with and without a plasma present in one arm of the interferometer. Typical runs of this sort are illustrated in Fig. VII-2b. Coupling the mechanical displacement of the driven grating with the X coordinate of the X-Y recorder and plotting on the Y coordinate the intensity of the signal from the Golay cell produces the Lissajous figure shown in Fig. VII-3 for two different indices of refraction, illustrating the change in shape of the figure which can be directly translated into a phase change that is due to the changing of the index of refraction.

A third method of reading the data which we also used was to design a mechanical linkage to the grating drive which was such that the phase could be adjusted by turning a knob. A run could then be taken with no plasma present, and with the plasma present the phase of the output of the Golay could be returned to its initial state, and the magnitude of the phase shift read directly as a phase angle on the mechanical linkage knob. It seemed a matter only of personal preference as to which of these three methods were to be used, since their accuracy seemed to be the same in each case.

A photograph of the complete system, including interferometer and necessary electronic equipment, is shown in Fig. VII-4.
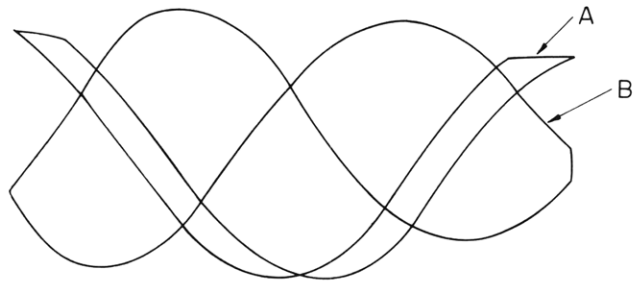
Fig. VII-3. Lissajous display of interferometer output. (X axis is grating position, Y axis is intensity.)

Fig. VII-4. Photograph of the complete system.

4. Results

The measurements of electron density were made in the positive column of a dc arc discharge in argon. The cylindrical discharge tube was 5 cm in diameter and 40 cm long. The two ends of the tube were closed off with crystal-quartz windows. The thermionically emitting, oxide-coated cathode and the water-cooled anode were situated in side arms of the main tube and thus allowed a clear optical path for the infrared radiation. Small Langmuir probes[7] were inserted at various places within the positive column.
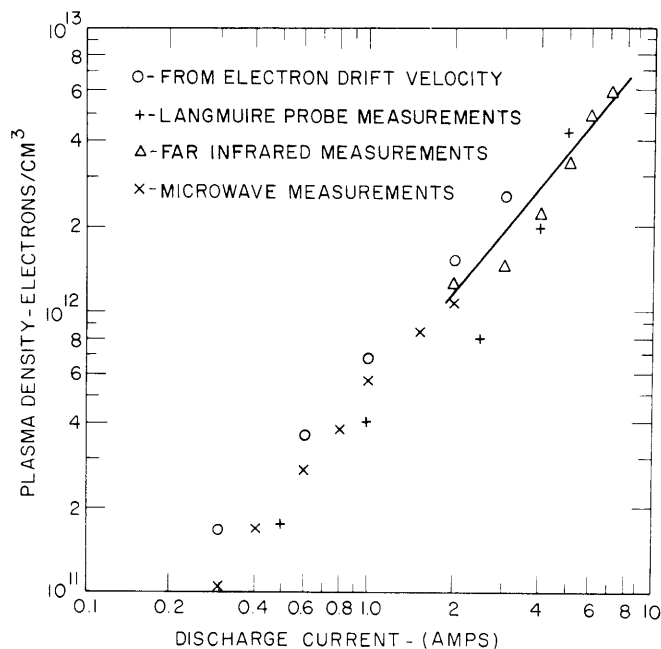

Fig. VII-5. Electron density as a function of discharge current.

Figure VII-5 shows a plot of the average electron density, deduced from infrared phase-shift measurements, as a function of the discharge current. We also measured the same plasma by using three other methods, the results of which are also shown in Fig. VII-5. The solid line is drawn through the triangular points corresponding to the infrared measurements. We see very good agreement between these measurements and results deduced from microwave interferometer measurements[8] made at a wavelength of 8 mm. Whereas the 8-mm measurements are beginning to approach the plasma resonant-frequency cutoff, and, therefore, become unreliable as one goes to high plasma densities, the infrared measurements begin approximately where the microwave method starts to fail and continues on up to really dense plasmas.

Illustrated in the figure are two other determinations of N. One refers to Langmuir probe measurements wherein N is deduced from the ion saturation current and from the electron temperature[7]; the other N is inferred from the axial voltage V, current density, and electron drift velocity[9] $v_d(V)$, through the relation $J = Ne\ v_d(V)$. It is obvious from the figure that these four methods are in agreement within the range of their overlap.

<div align="right">S. C. Brown, G. Bekefi, R. E. Whitney</div>

<div align="center">References</div>

1. V. L. Ginsburg, Propagation of Electromagnetic Waves in Plasma (Gordon and Breach, Science Publishers, Inc., New York, 1962).

2. R. A. Alpher and D. R. White, Phys. Fluids 1, 452 (1958).

3. M. J. E. Golay, Rev. Sci. Instr. 18, 357 (1947).

4. T. K. McCubbin, Jr., and W. M. Sinton, J. Opt. Soc. Am. 40, 537 (1950).

5. V. Roberts, Royal Radar Establishment, Malvern, England (private communication, letter dated March 9, 1962).

6. R. H. Dicke, Rev. Sci. Instr. 17, 268 (1946).

7. L. B. Loeb, Basic Processes of Gaseous Electronics (University of California Press, Berkeley, 1955), Chapter IV, Part 2.

8. J. M. Anderson and L. Goldstein, Technical Report No. 7, Electrical Engineering Research Laboratory, University of Illinois, Urbana, 1955; C. B. Wharton, UCRL Report No. 4836 (revised), Radiation Laboratory, University of California, 1957.

9. S. C. Brown, Basic Data of Plasma Physics (The Technology Press of M.I.T., Cambridge, Mass. and John Wiley and Sons, Inc., New York, 1959).

B. THEORY OF FAST-WAVE AMPLIFICATION OF MICROWAVES BY ELECTRONS

Several types of fast-wave interactions between electrons and electromagnetic radiation in the presence of a uniform magnetic field are analyzed with the help of a simplified physical model of the electron gas.

Theoretical predictions of amplification of electromagnetic waves traversing a nonthermal electron gas in the presence of an applied magnetic field have been given by several authors.[1-4] All of these authors considered the electrons as independent particles. Twiss,[1] and Bekefi, Hirshfield and Brown[2] relied on the Boltzmann transport equation in predicting a negative absorption coefficient. Bekefi, Hirshfield, and Brown also considered the particular case involving the relativistic velocity dependence of the electron mass. Schneider[3] used the relativistic Schrödinger equation to obtain the kinetic energy levels of an electron in a magnetic field. From this starting point, he derived conditions for amplification which can be shown, through application of the correspondence principle, to agree with those of Bekefi, Hirshfield, and Brown, and of Coccoli.[5,6]

Pantell and Chow[4] considered another type of fast-wave interaction that produces longitudinal bunching of an electron stream as a result of the interaction between the cyclotron motion of the electrons and the transverse rf magnetic field.

However, none of these approaches to the various interaction mechanisms seems to provide a simple, classical (as opposed to quantum), physical picture in which the individual electron behavior is apparent. Since these amplification mechanisms were predicted from an independent particle model, it seemed reasonable to hope that an analysis of the motion of a single electron in a magnetic field and interacting with an electromagnetic wave would exhibit the behavior that would lead to a basic understanding of the gain mechanism.

1. Equation of Motion of a Slightly Relativistic Electron in a Magnetic Field in the Presence of an Oscillating Electric Field

The equation of motion of an electron in an electromagnetic field is

$$\frac{d\vec{p}}{dt} = -e(\vec{E} + \vec{v} \times \vec{B}),\tag{1}$$

where

$$\vec{p} = m\vec{v} = \frac{m_0 \vec{v}}{(1-v^2/c^2)^{1/2}}\tag{2}$$

and m_0 is the electron rest mass.

The ac electric field is polarized in the x-direction. The uniform steady magnetic field is chosen in the z-direction. That is,

$$\vec{E} = \vec{i}_x E_1 \cos \omega t\tag{3}$$

$$\vec{B} = \vec{i}_z B_0.\tag{4}$$

Here, $\vec{i}_x$ and $\vec{i}_z$ are unit vectors in the x- and z-directions.

Only motion in a plane transverse to the magnetic field is considered here. The velocity vector is

$$\vec{v} = \vec{i}_x v_x + \vec{i}_y v_y\tag{5}$$

Equations 2 and 5 are combined to obtain

$$\frac{d\vec{p}}{dt} = \frac{m_0}{(1-v^2/c^2)^{1/2}}\left[\vec{i}_x \dot{v}_x\left(\frac{c^2 - v_y^2 + v_x v_y \frac{\dot{v}_y}{\dot{v}_x}}{c^2 - v^2}\right) + \vec{i}_y \dot{v}_y\left(\frac{c^2 - v_x^2 + v_x v_y \frac{\dot{v}_x}{\dot{v}_y}}{c^2 - v^2}\right)\right]\tag{6}$$

When the ac electric forces are much weaker than the steady magnetic force, that is, when $|eE_1| \ll |evB_0|$, the electron motion will be nearly circular, and $\dot{v}_z/\dot{v}_x \approx -v_x/v_y$. Equation 6 is then considerably simplified, and Eq. 1 may be written

$$\frac{m_0}{(1-v^2/c^2)^{1/2}} \, [\vec{i}_x \dot{v}_x + \vec{i}_y \dot{v}_y] = -e(\vec{E} + \vec{v} \times \vec{B}). \tag{7}$$

The components of Eq. 7 are

$$\frac{m_0 \dot{v}_x}{(1-v^2/c^2)^{1/2}} = -ev_y B_0 - eE_1 \cos \omega t \tag{8a}$$

$$\frac{m_0 \dot{v}_y}{(1-v^2/c^2)^{1/2}} = ev_x B_0. \tag{8b}$$

Equations 8a and 8b are combined to yield

$$\frac{m_0}{(1-v^2/c^2)^{1/2}} \, (v_x \dot{v}_x + v_y \dot{v}_y) = -ev_x E_1 \cos \omega t$$

or

$$\frac{1}{2} v \frac{dv}{dt} \approx -\frac{e}{m_0} (1-v^2/c^2)^{1/2} \, v_x E_1 \cos \omega t. \tag{9}$$

The velocity component v_x can be expressed in terms of v as

$$v_x = v \cos \phi(t) = v \cos \left[\phi_0 + \int_0^t \omega_b \, dt \right],$$

where ϕ is the initial phase between $\vec{v}$ and $\vec{E}_1$, and

$$\omega_b = \frac{e}{m} B_0 (1-v^2/c^2)^{1/2}. \tag{10}$$

Thus Eq. 9 becomes

$$\frac{dv}{dt} = -\frac{eE_1}{2m_0} (1-v^2/c^2)^{1/2} \left\{ \left[\cos \left(\omega t - \int_0^t \omega_b \, dt \right) + \cos \left(\omega t + \int_0^t \omega_b \, dt \right) \right] \cos \phi_0 \right.$$

$$\left. - \left[\sin \left(\omega t + \int_0^t \omega_b \, dt \right) - \sin \left(\omega t - \int_0^t \omega_b \, dt \right) \right] \sin \phi_0 \right\}. \tag{11}$$

In Eq. 11 the electric field has been resolved into left- and right-hand circularly polarized waves. The orbiting electrons are left-hand terms. The right-hand terms oscillate very rapidly and can be ignored. The slow variation in the electron

speed is given by

$$\frac{dv_{dc}}{dt} = -\frac{eE_1}{2m_o}\left(1 - \frac{v_{dc}^2}{c^2}\right)^{1/2}\left\{\cos\phi_o \cos\left(\omega t - \omega_{b_o}\int_0^t \left(1 - \frac{v_{dc}^2}{c2}\right)^{1/2} dt\right)\right.$$

$$\left. + \sin\phi_o \sin\left(\omega t - \omega_{b_o}\int_0^t \left(1 - \frac{v_{dc}^2}{c^2}\right)^{1/2} dt\right)\right\}.$$

(12)

2. Fast-Wave Interaction Based on Velocity Dependence of Electron Mass

The electron described by Eq. 12 initially emits or absorbs energy as prescribed by the phase ϕ_o. In a plasma or electron beam the phases ϕ_o are distributed randomly with equal probability. There are equal numbers of electrons in each of the four quadrants in velocity space. As a simplifying approximation, four representative types of electrons are chosen of charge density ne/4 and mass density nm/4, where n is the density of the electron gas. These four representative particles are initially spaced 90° from each other in velocity space. In the present calculation we have chosen $\phi_o = -\pi/2$, 0, $+\pi/2$, and π. The kinetic energy gained or lost per unit volume by these representative particles appears as loss or gain in the electromagnetic energy density. Since the present discussion is only concerned with the basic gain mechanism, encumbrances, such as electromagnetic energy losses at boundaries, and so forth, will be ignored.

The energy stored in the field is assumed to be of the form

$$U = \frac{1}{2}\epsilon E_1^2 \qquad \text{joules/meter}^3.$$

(13)

The change in the field energy is balanced by the change in kinetic energy density of the particles, that is,

$$\frac{dU}{dt} = \epsilon E_1 \frac{dE_1}{dt} = -\frac{n}{4}\sum_{\ell=1}^{4} \frac{d}{dt}(T)_\ell.$$

(14)

The kinetic energy of the ℓth electron is $T = m_\ell c^2 - m_o c^2$. Thus

$$\frac{n}{4}\frac{d}{dt}\sum (T)_\ell = \frac{n}{4}\sum_{\ell=1}^{4} \frac{m_o c^2}{\left(1 - v_\ell^2/c^2\right)^{3/2}}\left(\frac{v_\ell}{c}\right)\frac{d(v_\ell/c)}{dt}.$$

(15)

Equation 12 is substituted in Eq. 15, and the result is used with Eq. 14 to obtain a relation between the particle velocities and the ac electric field. This relation is

$$\frac{dE}{dt} = \frac{n}{4} \frac{ec}{\epsilon} \sum_{\ell=1}^{4} \frac{v_\ell/c}{1 - v_\ell^2/c^2} \cos\left[\omega t - \int_0^t \omega_{b_o} \left(1 - v_\ell^2/c^2\right)^{1/2} dt + \frac{\pi}{2}(\ell-1)\right]. \tag{16}$$

Equation 16 must be solved simultaneously with the equation of motion of the four representative particles. The five equations are put into the following dimensionless form

$$\frac{d\zeta_\ell}{d\tau} = -\mathcal{E} K\left(1-\zeta_\ell^2\right)^{1/2} \cos\left[W\tau - \int_0^\tau \left(1-\zeta_\ell^2\right)^{1/2} d\tau + \frac{\pi}{2}(\ell-1)\right], \qquad \ell = 1,2,3,4 \tag{17}$$

$$\frac{d\mathcal{E}}{d\tau} = \sum_{\ell=1}^{4} \frac{\zeta_\ell}{1 - \zeta_\ell^2} \cos\left[W\tau - \int_0^\tau \left(1-\zeta_\ell^2\right)^{1/2} d\tau + \frac{\pi}{2}(\ell-1)\right], \tag{18}$$

where

$$\zeta_\ell = v_{dc_\ell}^2 \Big/ c$$

$$W = \omega/\omega_{b_o}$$

$$\tau = w_{b_o} t$$

$$\mathcal{E} = 8\left(\frac{\omega_{b_o}^2}{\omega_P^2}\right)\frac{E_1}{cB_o}\frac{\epsilon}{\epsilon_o}.$$

$$\omega_P^2 = \frac{ne^2}{m_o \epsilon_o}$$

$$K = \frac{1}{16}\left(\frac{\omega_P^2}{\omega_{b_o}^2}\right)\frac{\epsilon_o}{\epsilon}.$$

The initial conditions at $\tau = 0$ are $\mathcal{E} = \mathcal{E}_o$ and $\zeta_\ell = \zeta_o$ (for $\ell = 1,2,3,4$).

3. Small-Signal Approximation to the Relativistic Fast-Wave Interaction Equation

Approximate solutions of Eqs. 17 and 18 can be obtained for values of τ for which

$$\left|W\tau - \int_0^\tau \left(1-\zeta_\ell^2\right)^{1/2} d\tau\right| \ll \frac{\pi}{2} \qquad \text{for } \ell = 1,2,3,4.$$

Under these conditions, Eq. 17 becomes

$$\frac{d\zeta_1}{d\tau} \approx -\mathscr{E}_o K \rightarrow \zeta_1 \approx \zeta_o - \mathscr{E}_o K\tau \tag{19}$$

$$\frac{d\zeta_2}{d\tau} \approx +\mathscr{E}_o K\left(1-\zeta_o^2\right)^{1/2}\left[W-\left(1-\zeta_o^2\right)^{1/2}\right]\tau \rightarrow \zeta_2 \approx \zeta_o + A\tau \tag{20}$$

$$\frac{d\zeta_3}{d\tau} \approx \mathscr{E}_o K \rightarrow \zeta_3 \approx \zeta_o + \mathscr{E}_o K\tau \tag{21}$$

$$\frac{d\zeta_4}{d\tau} \approx -\mathscr{E}_o K\left(1-\zeta_o^2\right)^{1/2}\left[W-\left(1-\zeta_o^2\right)^{1/2}\right]\tau \rightarrow \zeta_4 \approx \zeta_o - A\tau \tag{22}$$

where

$$A = \frac{1}{2}\mathscr{E}_o K\left[W-\left(1-\zeta_o^2\right)^{1/2}\right]\left(1-\zeta_o^2\right)^{1/2}.$$

The small-signal condition is

$$\mathscr{E}_o K\tau \ll \zeta_o, \quad A\tau \ll \zeta_o. \tag{23}$$

Equations 19-22 are substituted in Eq. 18.

The pair of electrons (2 and 4) with initial phases $-\pi/2$, $+\pi/2$ contribute a term to the change in the ac electrical field

$$\left.\left|\frac{d\mathscr{E}}{d\tau}\right|\right)_{2,4} \approx \mathscr{E}_o K\left[W-\left(1-\zeta_o^2\right)^{1/2}\right]\left[\left(1-\zeta_o^2\right)^{1/2}-\frac{1}{3}\zeta_o^2-W\right]\tau^3. \tag{24}$$

This expression is positive in the narrow range

$$\left[\left(1-\zeta_o^2\right)^{1/2}-\frac{1}{3}\zeta_o^2\right] < W < \left(1-\zeta_o^2\right)^{1/2} \qquad \text{for all } \tau.$$

Thus, $\Delta\omega \sim (v/c)^2 \omega_{b_o}$.

The second pair of electrons (1 and 3) with initial phases $0, \pi$ contribute a term

$$\left.\left|\frac{d\mathscr{E}}{d\tau}\right|\right)_{1,3} \approx -2\mathscr{E}_o K\tau. \tag{25}$$

The ratio of (24) and (25) is

$$\frac{(d\mathscr{E}/d\tau)_{2,4}}{(d\mathscr{E}/d\tau)_{1,3}} \sim \zeta_o^4\tau^2. \tag{26}$$

In order to obtain amplification, $\zeta_o^4\tau^2$ must be greater than 1. If the electron is present in the interaction region for a time $t = 1/\nu$, we obtain from Eq. 26

$$\left(\frac{v}{c}\right)^2 > \frac{\nu}{\omega_b{}_o},$$

a condition that has been given elsewhere.[3, 5, 6]

4. Equations of Motion of a Nonrelativistic Electron in a Magnetic Field Including Interactions with the RF Magnetic Field

The equations of motion of an electron in the uniform magnetic field, $\vec{i}_z B_o$, in the presence of an electromagnetic wave propagating in the direction of the magnetic field and with the ac electric vector in the x-direction are:

$$m\dot{v}_x = qE_1 \cos\left[\omega t - \frac{2\pi}{\lambda} \int_0^t v_z \, dt - \frac{2\pi z_o}{\lambda}\right] + qv_y B_o \tag{27}$$

$$m\dot{v}_y = -qv_x B_o \tag{28}$$

$$m\dot{v}_z = qv_x B_1 \cos\left[\omega t - \frac{2\pi}{\lambda} \int_0^t v_z \, dt - \frac{2\pi z_o}{\lambda}\right]. \tag{29}$$

It is assumed that $v_z \ll v_x, v_y$. The term

$$\frac{2\pi}{\lambda} \int_0^t v_z \, dt = \frac{2\pi(z-z_o)}{\lambda}$$

accounts for the change in phase between the electron velocity and the ac fields as the z component of the electron changes.

Equations 27 and 28 can be combined to obtain

$$m\left[v_x \frac{dv_x}{dt} + v_y \frac{dv_y}{dt}\right] = qE_1 v_x \cos\left[\omega t - \frac{2\pi}{\lambda} \int_0^t v_z \, dt - \frac{2\pi z_o}{\lambda}\right]. \tag{30}$$

Since the longitudianl forces are much weaker than the traverse forces acting on the electrons, it can be assumed that

$$\frac{d}{dt}\left(\frac{1}{2} mv^2\right) \approx \frac{d}{dt}\left(\frac{1}{2} mv_T\right)^2,$$

where $v_T^2 = v_x^2 + v_z^2$. Thus,

$$\frac{d}{dt}\left(\frac{1}{2} mv^2\right) \approx m\left[v_x \frac{dv_x}{dt} + v_y \frac{dv_y}{dt}\right] = mv \frac{dv}{dt}. \tag{31}$$

The assumptions and approximations above can be used to approximate v_x by

$$v_x \approx v \cos\left[\omega_b t + \phi_o\right]. \tag{32}$$

With the approximation of Eqs. 31 and 32, Eqs. 29 and 30 become

$$\frac{dv}{dt} = \frac{q}{m} E_1 \cos (\omega_b t + \phi) \cos \left[\omega t - \frac{2\pi}{\lambda} \int_0^t v_z \, dt - \frac{2\pi z_o}{\lambda} \right]$$

$$\frac{dv_z}{dt} = \frac{q}{m} B_1 v \cos (\omega_b t + \phi_o) \cos \left[\omega t - \frac{2\pi}{\lambda} \int_0^t v_z \, dt - \frac{2\pi z_o}{\lambda} \right].$$

The trigonometric terms are combined and the right-hand circularly polarized wave is neglected, as in section 1. The slower variations in the electron's speed are given by

$$\frac{dv_{dc}}{dt} = \frac{q}{2m} E_1 \cos \left[(\omega_b - \omega')t + \frac{\omega}{v_p} \int_0^t V_{z_{dc}} \, dt + \phi_1 \right]$$

$$\frac{dV_{z_{dc}}}{dt} = \frac{q}{2m} B_1 v_{dc} \cos \left[(\omega_b - \omega')t + \frac{\omega}{v_p} \int_0^t V_{z_{dc}} \, dt + \phi_1 \right], \tag{33}$$

where

$$V_z = v_z - v_{z_o}$$

$$\omega' = \omega \left(1 - \frac{v_{z_o}}{v_p} \right)$$

v_p = wave phase velocity in the z-direction

$$\phi_1 = \phi_o + \frac{2\pi z_o}{\lambda}.$$

5. Fast-Wave Interaction and Small-Signal Analysis

As before, the change in kinetic energy of the four representative electrons is balanced with the change in field energy. The following dimensionless equations result.

$$\frac{d\mathcal{E}}{d\tau} = -\sum_{\ell=1}^{4} \zeta_\ell \cos\left[W'\tau + w\int_0^\tau \xi_\ell \, d\tau + \frac{\pi}{2}(\ell-1)\right] \tag{34}$$

$$\frac{d\zeta_\ell}{d\tau} = K_1 \mathcal{E} \cos\left[W'\tau + w\int_0^\tau \xi_\ell \, d\tau + \frac{\pi}{2}(\ell-1)\right] \qquad \ell = 1, 2, 3, 4 \tag{35}$$

$$\frac{d\xi_\ell}{d\tau} = K_2 \zeta_\ell \mathcal{E} \cos\left[W'\tau + w\int_0^\tau \xi_\ell \, d\tau + \frac{\pi}{2}(\ell-1)\right] \qquad \ell = 1, 2, 3, 4, \tag{36}$$

where

$$\mathcal{E} = 8\left(\frac{\omega_b^2}{\omega_P^2}\right)\frac{\epsilon}{\epsilon_o}\frac{E_1}{B_o c}$$

$$\zeta = v_{dc}/c$$

$$\xi = V_{z_{dc}}/c$$

$$\tau = \omega_b t$$

$$W' = 1 - \omega'/\omega_b$$

$$w = \frac{\omega}{\omega_b} \cdot \frac{c}{v_p}$$

$$K_1 = \frac{1}{16}\left(\frac{\omega_P^2}{\omega_b^2}\right)\left(\frac{\epsilon_o}{\epsilon}\right)$$

$$K_2 = \frac{B_1 c}{E_1} K_1.$$

When

$$W\tau + w\int_0^\tau \xi_\ell \, d\tau \ll \frac{\pi}{2},$$

Eqs. 35 and 36 are approximated as follows: $\tag{37}$

$$\frac{d\xi_1}{d\tau} \approx K_2\zeta_o\mathscr{E}_o \rightarrow \xi_1 \approx K_2\zeta_o\mathscr{E}_o\tau$$

$$\frac{d\xi_2}{d\tau} \approx -K_2\zeta_o\mathscr{E}_oW'\frac{\tau^2}{2} \rightarrow \xi_2 \approx -K_2\zeta_o\mathscr{E}_oW'\frac{\tau^3}{6}$$

$$\frac{d\xi_3}{d\tau} \approx -K_2\zeta_o\mathscr{E}_o \rightarrow \xi_3 \approx -K_2\zeta_o\mathscr{E}_o\tau \tag{38}$$

$$\frac{d\xi_4}{d\tau} \approx K_2\zeta_o\mathscr{E}_oW'\frac{\tau^2}{2} \rightarrow \xi_4 \approx K_2\zeta_o\mathscr{E}_oW'\frac{\tau^3}{6}$$

$$\frac{d\zeta_1}{d\tau} \approx K_1\mathscr{E}_o \rightarrow \zeta_1 \approx \zeta_o + K_1\mathscr{E}_o\tau$$

$$\frac{d\zeta_2}{d\tau} \approx -K_1\mathscr{E}_oW'\tau \rightarrow \zeta_2 \approx \zeta_o - K_1 {}_oW'\frac{\tau^2}{2}$$

$$\frac{d\zeta_3}{d\tau} \approx -K_1\mathscr{E}_o \rightarrow \zeta_3 \approx \zeta_o - K_1\mathscr{E}_o\tau \tag{39}$$

$$\frac{d\zeta_4}{d\tau} \approx K_1 {}_oW'\tau \rightarrow \zeta_4 \approx \zeta_o + K_1 {}_oW'\frac{\tau^2}{2}$$

The pair of electrons, 1 and 3, contribute

$$\left(\frac{d\mathscr{E}}{d\tau}\right)_{1,3} \approx K_2\mathscr{E}_o\zeta^2W'w\left[\tau^3 + \frac{K_1}{K_2}\frac{W'}{w}\frac{\tau^2}{\zeta_o^2} - \frac{2K_1}{W'wK_2}\frac{\tau}{\zeta_o^2}\right]$$

$$\approx K_2\mathscr{E}_o\zeta_o^2W'w\tau^3. \tag{40}$$

The pair of electrons, 2 and 4, contribute

$$\left(\frac{d\mathscr{E}}{d\tau}\right)_{2,4} \approx -K_2\mathscr{E}_o\zeta_o^2W'w\tau^3\left[\frac{1}{3} + \frac{K_1W'}{wK_2\zeta_o^2}\right]. \tag{41}$$

Therefore, for net amplification

$$\frac{K_1}{wK_2}\frac{W'}{\zeta_o^2} < \frac{2}{3} \tag{42}$$

or

$$\omega_b - \omega' < \frac{2}{3}\omega\left(\frac{v_T}{v_p}\right)^2.$$

Thus, the bandwidth is comparable to that given in section 3 for the relativistic mechanism. The term W' in Eq. 40 must be positive for gain to occur, which is in agreement with the "slippage" conditions of Chow and Pantell.[4] Thus, $0 < \omega_b - \omega' < \frac{2}{3}\omega(v_T/v_p)$. The bandwidth is comparable to that found in the relativistic case discussed in section 3.

It has been possible by using four representative electrons to obtain many of the features of the fast-wave mechanisms. These are:

(a) The narrow bandwidth, proportional to $(v/c)^2$ for the relativistic mechanism, and proportional to $(v/v_p)^2$ for the ac magnetic interaction.

(b) The minimum radiation-time condition for the relativistic case $(v/c)^2 > v/\omega_{b_o}$.

(c) The slippage condition for both mechanisms.

<div align="right">J. D. Coccoli</div>

References

1. R. Q. Twiss, Australian J. Phys. 11, 564 (1958).

2. G. Bekefi, J. L. Hirshfield, and S. C. Brown, Phys. Fluids 2, 173 (1961).

3. J. Schneider, Phys. Rev. Letters 2, 504 (1959).

4. K. K. Chow and R. H. Pantell, A Small Signal Analysis of the Electron Cyclotron Backward Wave Oscillator, Microwave Laboratory Report 851, Stanford University, Stanford, California, October 1961.

5. J. D. Coccoli, Synchrotron radiation and negative absorption by nonthermal electrons in a magnetic field, Quarterly Progress Report No. 60, Research Laboratory of Electronics, M.I.T., January 15, 1961, pp. 13-17.

6. J. D. Coccoli, Study of Plasma Amplifiers, Final Report on Contract AF19(604)-8372, Microwave Associates, Burlington, Massachusetts, April 30, 1962.